Using SEMAC at 3 T MR to evaluate spinal metallic implants and peripheral soft tissue lesions

Chun Xin, MB[a], Houdong Liu, MS[a], Shihong Li, PhD, MD[b,*], Guangwu Lin, PhD, MD[b,*]

Abstract

We aimed to assess the usefulness of slice-encoding metal artifact correction (SEMAC) for the evaluation of spinal metallic implants and peripheral soft tissue lesions at 3T magnetic resonance.

Twenty-seven patients with spinal metal implants underwent both SEMAC and high bandwidth (HiBW) based sequences scanning for reduction artifacts. The area size and maximum longitude of artifacts, the peri-prosthetic soft tissue, and metal visualization were assessed by 2 independent doctors, as well as the lesions signs were reviewed by 2 senior readers. A paired 2-tailed t-test and McNemar test were used for statistical analysis.

The size of artifacts on SEMAC images decreased by 37% and 24%, and the scores are higher than that on HiBW images. T_1 weighted (T_1W)-SEMAC acquired the highest score in metal prosthesis visualization, while short tau inversion recovery SEMAC showed more signs of lesions than clinical HiBW group.

SEMAC effectively reduces the metal artifacts and is useful for assessing soft tissue lesions.

Abbreviations: Gd-DTPA = gadolinium diethylene triamine pentacetic acid, HiBW = high bandwidth, MR = magnetic resonance, MRI = magnetic resonance imaging, ROI = region of interest, SEMAC = slice-encoding metal artifact correction, STIR = short tau inversion recovery, T_1W = T_1 weighted, T_2W = T_2 weighted, TSE = turbo spin echo, VAT = view-angle tilting.

Keywords: high bandwidth, magnetic resonance imaging, metal artifact, metal visualization, metallic implants, slice-encoding metal artifact correction, view-angle tilting

1. Introduction

Vertebral fractures are typically caused by major trauma, particularly those that occur in osteoporosis patients. Such fractures can directly lead to secondary spinal cord and periphery soft tissues damage.[1] Operation treatment is aimed at decompressing the vertebral canal and stabilizing the disrupted

centrums. Thus, metallic implants, such as pedicle screws, are often used in orthopedic surgery to fixate the fractures to align and immobilize the vertebra. However, some complications can still occur after the operation, including infections, neural deficits, and Brown–Séquard syndrome, which may affect the prognosis of the patients.[2–4]

At present, X-ray plain radiographs and computed tomography scanning are 2 routine tools that are used in the assessment of spinal metal prostheses during the perioperation.[5,6] However, X-ray plain radiographs provide little information regarding physical characteristics, which are based on the natural contrast between the implant metal and human structures. Although computed tomography imaging with the 2-dimensional cross-sectional method and raw data can be reconstructed into 3-D images, which will provide better images, the metal-induced streak/beam-hardening artifacts still contaminate the data around the metal implants. Subsequently, these 2 methods are not sensitive for imaging the soft tissue complications around the implants, such as bone marrow lesions, infections, and edemas.[7]

Magnetic resonance imaging (MRI) is one of the most sensitive tools for detecting lesions of soft tissues due to its higher contrast in different sequences, potentially without any contrast media. However, metallic implants can cause local magnetic field inhomogenous, which cause the MRI images to suffer from severe artifacts, including signal loss and blurring.[8] Traditionally, the distortion of MRI with metal implants can be categorized as through-plane or in-plane distortions.[9] The use of thin slices and high bandwidth (HiBW), both for radiofrequency pulses and signal readout, has been suggested as an option to partially reduce these distortions. Recently, some MRI acquisition techniques were developed to reduce the artifacts of metal in

Table 1

Two groups of different imaging sequences.

SEMAC group (researched)	HiBW group (controlled)
STIR-SEMAC	STIR-HiBW
T_1W-SEMAC	T_1W-HiBW

HiBW = high bandwidth, SEMAC = slice encoding metal artifact correction, STIR = short time inversion recovery, T_1W = T_1-weighted imaging.

the body. In 1988, the view-angle tilting (VAT) technique was first introduced to correct in-plane distortions[10]; however, this technique cannot resolve through-plane distortions.[7] To resolve this problem, the advanced magnetic resonance (MR) techniques of slice- encoding metal artifact correction (SEMAC) and multi-acquisition variable-resonance image combination have been proposed to minimize the artifacts near metallic prostheses.[7,11–14] By extending the VAT turbo spin echo (TSE) with an additional phase-encoding along the slice-selective z-axis, SEMAC uses a TSE acquisition mode to correct the profiles of each excited slice in the region. The resolved profiles of all slices in the region of interest (ROI) are aligned to their actual voxel locations to resolve through-slice distortions.[7]

In this study, we aimed to assess the spinal metallic implants and peripheral soft tissues with SEMAC using a 3 T MR scanner, and to evaluate the clinical value of SEMAC in spinal metal prostheses comparing with clinical HiBW sequences.

2. Materials and methods

2.1. General information of the subjects

This prospective study was approved by our Institutional Review Board and performed between January 2015 and December 2017. We established the following inclusion criteria: patients with a history of spinal fixation surgery, limb paralysis, lower back pain, and other local symptoms or with a history of tumor in the surgical region; patients also had to provide informed consent. The exclusion criteria were patients with a cardiac pacemaker or who had major complications; who cannot bear to complete the scanning; and who are allergic to the contrast agent.

Thirty-three patients with metallic prostheses after spinal surgery were recruited for this research, and 27 patients met the inclusion criteria (15 females and 12 males). The average age was 61.6 ± 11.3 years. The average fixation segments were 2.52 levels: 2 segments of 17 patients, 3 segments of 6 patients, and 4 segments of 4 patients. Postoperative MRI was performed in 6 conditions:

(1) back pain without disc herniation recurrence (n=9),
(2) back pain with other-level herniated nucleus pulposus (n=7),
(3) postoperative evaluation of intraspinal tumors (n=6),
(4) back pain with sequelae of compression fracture (n=3),
(5) back pain with a fresh compression fracture (n=1), and
(6) fever evaluation (n=1).

2.2. MRI protocols

All MRI examinations were performed on a 3 T MRI scanner (MAGNETOM Skyra, Siemens Healthcare, Erlangen, Germany) using an integrated spine coil. SEMAC sequences were proto-types provided by Siemens Healthcare. Short tau inversion recovery (STIR) sequence and T_1W TSE with and without the advanced SEMAC techniques were prescribed to image metals in the patient spines (see Table 1), and the generalized autocalibrating partially parallel acquisition technique was used in the SEMAC group to reduce the total acquisition time. The parameters of the SEMAC and HiBW sequences are summarized in Table 2.

2.3. Data analysis

In the coronal images, 2 fellowship-trained radiologists drew ROIs of the axial pedicle screws, which included the blurring and signal loss regions to measure the size of the metallic artifacts. Two radiologists performed a semi-quantitative assessment of the prosthesis and peripheral soft tissues. The patients' information and imaging parameters were hidden to minimize the learning bias. Two experienced musculoskeletal radiologists (Prof Ji and Dr Lin, with 35 and 16 years of experience in the interpretation of spinal MRI, respectively) analyzed the different imaging findings of all of the in vivo data, and the positive signs were recorded.

Table 2

Imaging parameters of the 2 groups.

	STIR-SEMAC	STIR-HiBW	T_1W-SEMAC	T_1W-HiBW
TR/TE (ms)	7500/38	7200/43	800/11	774/14
TI (ms)	220	220	/	/
FA	140	140	140	140
TA	~10'	~3'38"	~8'22"	~2'04"
FOV (mm)	280	280	280	280
Matrix	256 × 256	256 × 256	384 × 384	384 × 384
Average	1	1	1	1
Number of slices	25	25	25	25
Thickness/distance factor (%)	3/0	3/0	3/0	3/0
Voxel dimensions (mm)	1.1 × 1.1 × 3	1.1 × 1.1 × 3	0.7 × 0.7 × 3	0.7 × 0.7 × 3
BW (Hz/Px)	673	673	685	685
SEMAC encoding steps	8	0	8	0
VAT	on	off	on	off
Parallel acquisition technique mode	GRAPPA, x3	off	GRAPPA, x2	off

BW = bandwidth, FA = flip angle, FOV = field of view, GRAPPA = generalized autocalibrating partially parallel acquisitions, HiBW = high bandwidth, SEMAC = slice-encoding metal artifact correction, STIR = short tau inversion recovery, T_1W = T_1-weighted imaging, TA = acquisition time, TE = echo time, TI = inversion time, TR = repetition time, VAT = viewing angle tilting.

Table 3

Sizes of the axial artifacts of 102 pedicle screws.

Screws (n = 102)	STIR-SEMAC	STIR-HiBW	Decrease (%)	P-value
Area (cm^2)	1.10 ± 0.09	1.74 ± 0.40	36.95%	<.000
Length (cm)	1.50 ± 0.19	1.96 ± 0.39	23.80%	<.000

HiBW = high bandwidth, SEMAC = slice encoding metal artifact correction, STIR = short time inversion recovery.

We referenced the literature to establish a semi-quantitative standard to assess the effect of the sequences on reducing the metal artifacts and usefulness for clinical diagnosis. Five imaging findings of periprosthetic tissues and prosthetic regions were evaluated, including:

a) the structures in vertebral canal, such as the dural sac, spinal cord, and cauda equine,
b) the intervertebral neural foramens,
c) the implant interface (bone marrow, muscles),
d) the intervertebral disc between the affected intervertebral disc level, and
e) overall artifacts.

They were assessed using 5-point scales as follows[15,16]:

(1) A grade of 1 indicated the worst quality for interpretation, where the periprosthetic region was barely delineated; a grade of 2 indicated visualization of less than 25% of the aforementioned structures; a grade of 3 indicated visualization of 25% to 50% of the structures; a grade of 4 indicated visualization of 50% to 75% of the structures; and a grade of 5 indicated visualization of more than 75% of the structures. With the cross-reference function, axial images that were obtained at the level of the center of the pedicle screws were selected for evaluation of visibility of the dural sac, visibility of the bone-implant interface and overall artifacts. Axial images just below the pedicles or the coronal images were selected for evaluation on the visibility of neural foramens.
(2) Metallic prostheses, which were delineated by a dark signal intensity with clearly marginated prosthetic contours, were graded as follows: a grade of 1 indicated nearly complete non-visualization of the prosthesis; a grade of 2 indicated visualization of less than one third of the prosthesis; a grade of 3 indicated visualization of one to two thirds of

the prosthesis; a grade of 4 indicated visualization of more than two thirds of the prosthesis; and a grade of 5 indicated that the entire prosthesis was delineated and free of artifacts.

2.4. Statistical analysis

The data were recorded using Excel 2013 (Microsoft Corporation) and analyzed using software IBM SPSS (Statistical Package for Social Sciences) Statistics version 21.0 for Windows. The screw artifact sizes between 2 imaging groups were compared using a paired samples t-test, and the semi-quantitative scores of the 2 group images were obtained using a paired samples t-test. A comparison of the abnormal signs from different sequences was performed using the McNemar test for the matched data.

3. Results

3.1. Quantitative evaluation of metal artifacts

The Dice index for ROIs drawn by the 2 fellowship-trained radiologists was 0.82 ± 0.03. The areas of the pedicle screws are shown in Table 3. The area of the SEMAC group decreased by 36.95% compared to the traditional HiBW group, and the maximum artifact length decreased by 23.8%.

3.2. Semi-quantitative evaluation of metal artifacts

The k's Cohen for the 2 experienced radiologists was 0.84 ± 0.04. The semi-quantitative assessment for peri-prosthetic tissues showed that the STIR-/T$_1$W-SEMAC scores were significantly higher than those of the clinical HiBW group ($P < .05$) (Table 4). Figure 1 shows the metal prosthesis visualization scores in 4 sequences from 2 radiologists. The scores in descending order were T$_1$W-SEMAC > STIR-SEMAC > T$_1$W-HiBW > STIR-HiBW, and the scores of T$_1$W-SEMAC were significantly higher than other groups.

3.3. Positive signs

Table 5 provides a comparison of the positive signs between 2 different STIR sequences from 2 observers. Significantly, more bone marrow lesions, herniated intervertebral discs, intervertebral foramen and radiculitis, and soft tissue edemas were detected

Table 4

Semi-quantitative assessment for peri-prosthetic tissues.

	Radiologist A			Radiologist B		
STIR	SEMAC	HiBW	P-value	SEMAC	HiBW	P-value
Dural sac / spinal cord / cauda equine	2.59 ± 0.57	1.70 ± 0.47	.000	3.04 ± 0.44	1.74 ± 0.45	.000
Intervertebral neural foramens / nerve root	2.85 ± 0.60	1.78 ± 0.42	.000	3.30 ± 0.54	1.85 ± 0.36	.000
Bone marrow / muscles	2.70 ± 0.72	1.74 ± 0.45	.000	2.93 ± 0.68	1.70 ± 0.47	.000
Intervertebral disc	3.03 ± 0.65	1.81 ± 0.56	.000	3.04 ± 0.65	1.85 ± 0.36	.000
overall Artifacts	2.70 ± 0.78	1.63 ± 0.49	.000	2.81 ± 0.62	1.67 ± 0.48	.000
T$_1$W	**SEMAC**	**HiBW**	**P-value**	**SEMAC**	**HiBW**	**P-value**
Dural sac / spinal cord / cauda equine	2.74 ± 0.53	2.04 ± 0.52	.000	2.89 ± 0.42	2.15 ± 0.36	.000
Intervertebral neural foramens / nerve root	2.96 ± 0.59	2.25 ± 0.34	.000	3.56 ± 0.58	1.93 ± 0.27	.000
Bone marrow / muscles	3.0 ± 0.48	2.19 ± 0.62	.000	3.26 ± 0.53	2.0 ± 0.48	.000
Intervertebral disc	2.59 ± 0.50	1.93 ± 0.73	.000	3.19 ± 0.68	1.78 ± 0.42	.000
Overall artifacts	2.96 ± 0.44	2.04 ± 0.59	.000	3.11 ± 0.42	1.81 ± 0.48	.000

HiBW = high bandwidth, SEMAC = slice encoding metal artifact correction, STIR = short tau inversion recovery, T$_1$W = T$_1$-weighted imaging.

Metal prosthesis visualization
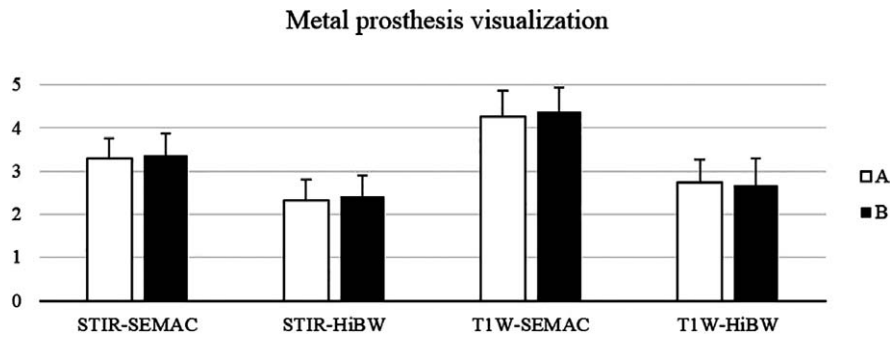
Figure 1. shows a comparison of the semi-quantitative evaluation scores of metal prostheses; T_1 weighted slice-encoding metal artifact correction has a higher score than the other sequences.

in the STIR-SEMAC group than in the clinical HiBW group. In addition, there were more positive signs in the STIR-SEMAC group than in the STIR-HiBW group.

Table 6 shows that there were more instances of peri-prosthetic osteolysis and soft tissue edemas in T_1W-SEMAC than in the T_1W-HiBW group, and there were significant differences between the 2 groups. Moreover, there were more positive signs in the T_1W-SEMAC group than in the T_1W-HiBW group.

3.4. Case interpretation

A 46-year-old male with spinal fixation is shown in Figure 2. Picture A was imaged with fat saturation prepared T_2 weighted (T_2W) TSE, and the surgical area shows ripple-like metal artifacts blurring the peripheral soft tissues, which makes it difficult to evaluate the condition. Picture B was imaged with STIR-HiBW, and picture C was imaged with STIR-SEMAC. We can observe a large range of exudation and effusion around the cross-link

Table 5

Comparison of positive signs between 2 different STIR sequences.

STIR	Radiologist A			Radiologist B		
	SEMAC	HiBW	*P-value*	SEMAC	HiBW	*P-value*
Bone marrow lesions	12	3	*.004*	13	2	*.001*
Herniated Intervertebral Disks	9	4	*.063*	9	4	*.063*
Spinal stenosis	6	4	*1*	5	4	*1*
Intervertebral foramen and Radiculitis	11	5	*.031*	14	7	*.016*
Facet joint changes	7	2	*.063*	5	2	*.25*
Compression fractures	4	4	*1.0*	4	4	*1.0*
Tumors	6	5	*1.0*	6	6	*1.0*
Postoperative infection	2	2	*1.0*	2	2	*1.0*
Soft-tissue edema	23	14	*.041*	18	11	*.016*
Others	7	3	*.125*	6	2	*.125*
Total	87	45		82	44	

HiBW = high bandwidth, SEMAC = slice encoding metal artifact correction, STIR = short tau inversion recovery.

Table 6

Comparison of the positive signs between 2 different T_1W sequences.

| T_1W	Radiologist A			Radiologist B		
	SEMAC	HiBW	*P-value*	SEMAC	HiBW	*P-value*
Alignment disorders	5	5	*1.0*	5	5	*1.0*
Bone marrow lesions	4	1	*.25*	4	1	*.25*
Herniated intervertebral disk	7	4	*.25*	6	4	*.5*
Spinal stenosis	5	4	*1.0*	4	5	*1.0*
Intervertebral foramen and radiculitis	7	5	*.5*	8	6	*.5*
Changes of the posterior elements	4	1	*.25*	3	1	*.5*
Compression fractures	4	3	*1.0*	5	5	*1.0*
Tumors	6	4	*.5*	6	4	*0.5*
Postoperative infection	1	0	*NA*	1	0	*NA*
Soft-tissue edema	9	3	*.031*	7	2	*.063*
Periprosthetic osteolysis	11	4	*.016*	13	4	*.004*
Others	5	2	*.25*	6	3	*.25*
Total	68	37		68	40	

HiBW = high bandwidth, SEMAC = slice-encoding metal artifact correction, T_1W = T_1-weighted imaging.
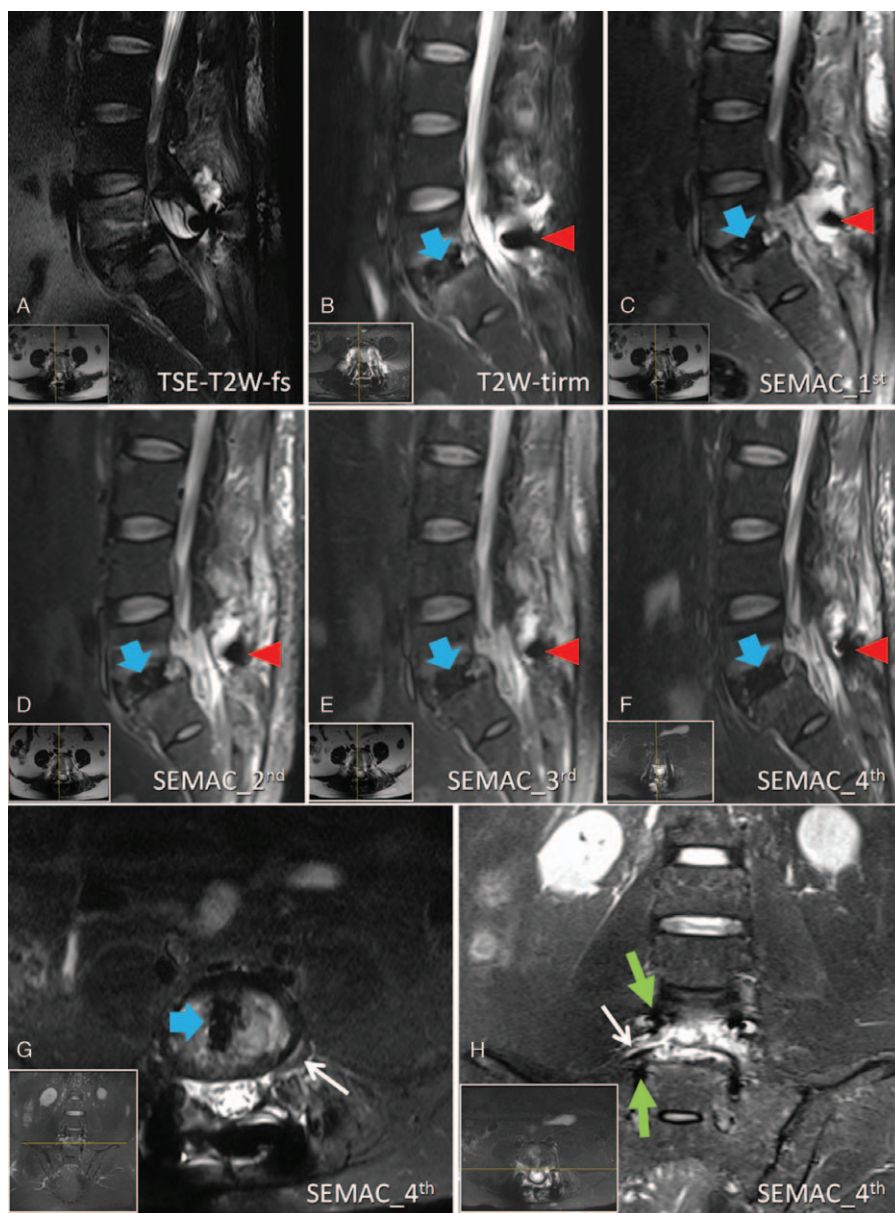
Figure 2. A 46-year-old male with spinal fixation subjected to magnetic resonance imaging (MRI) scanning 4 times for fever evaluation. Pictures A–C are the first MRI examination. Picture A is an image obtained with the traditional turbo spin echo sequence combined with selected fat saturation, where the surgical area shows ripple-like metal artifacts. Picture B was imaged with short tau inversion recovery -high bandwidth, and picture C was imaged with short tau inversion recovery-slice-encoding metal artifact correction. There was considerable exudation and effusion around the cross-link device in picture C (red arrows), and the metal artifacts were decreased compared to A and B. Pictures D–F are the subsequent weekly follow-up images with short tau inversion recovery-slice-encoding metal artifact correction. In this 4-week period, antibiotics were used moderately, and the exudation surrounding the implanted metals, bone marrow edema, and soft tissue swelling were successively alleviated as reflected in the MRI. The white arrows in pictures G and H indicate the nerve roots running out from the unilateral intervertebral foramens. Slight visible effusion in the nerve root sheath sleeve can be observed. The green arrows indicate the pedicle screws.

device in picture C, and the metal artifacts were decreased compared to pictures A and B. Pictures D–F are the subsequent weekly follow-up images with STIR-SEMAC. In this 4-week period, antibiotics were used moderately, and the exudation surrounding the implanted metals, bone marrow edema, and soft tissue swelling were successively alleviated as reflected in the MRI. The white arrows in pictures G and H indicate the nerve roots running out from the unilateral intervertebral foramens, with slight visible effusion in the nerve root sheath sleeve shown; the green arrows indicate the pedicle screws.

A 73-year-old male patient is shown in Figure 3. Pictures A and B were preoperative sagittal fat-suppressed T_2W and axial fat-suppressed T_1W with gadolinium diethylene triamine pentacetic acid (Ga-DTPA enhancement images obtained approximately 3 years ago respectively. Picture A shows bone destruction in several cervical vertebral bodies and accessories at the level of C2–4. In addition, it illustrates spinal stenosis and soft tissue in the epidural space. Picture B shows lesions in the vertebral body, accessories, intraspinal epidural soft tissues, and the para-vertebral soft tissue were significantly enhanced, with expansion
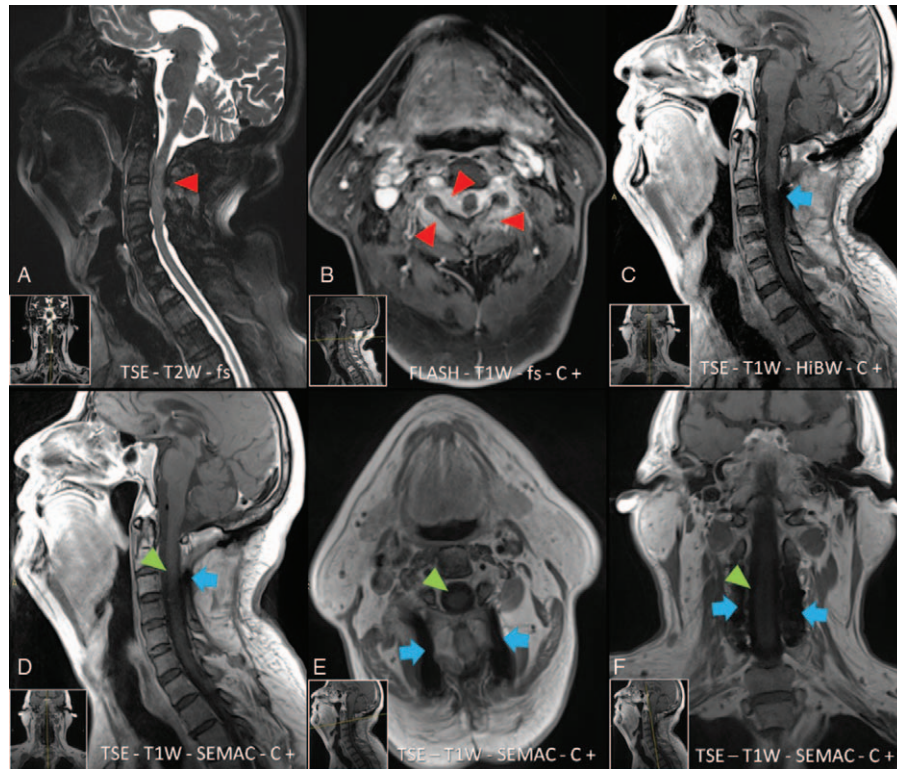
Figure 3. A diffuse large B cell lymphoma patient. Pictures A and B were preoperative sagittal fat-suppressed T_2 weighted and axial fat-suppressed T_1 weighted with Gd-DTPA enhancement images taken approximately 3 years ago. Picture A shows bone destruction in several cervical vertebral bodies and accessories at the level of C2–4. Spinal stenosis and soft tissue in the epidural space are also observed. Picture B shows that lesions in the vertebral body, accessories, intraspinal epidural soft tissues, and the paravertebral soft tissue were significantly enhanced, with expansion of the right intervertebral foramen and compressed spinal cord (lesions pointed by red arrows). Pictures D–F are images of enhanced T_1 weighted with slice-encoding metal artifact correction and view-angle tilting, where the metal artifacts (blue arrows) are narrower than in Picture C. The spinal cord is indicated by the green arrows.

of the right intervertebral foramen, and compressed spinal cord. We considered a diagnosis of a malignant tumor (i.e., lymphoma, metastasis). The lesions were observed, as indicated by the red arrows.

Next, the patient underwent a hollow needle biopsy at Fudan University Shanghai Cancer Center, and a pathological smear was observed. A large number of lymphocytes and some atypical cells were observed, and non-Hodgkin lymphoma was considered. On January 5, 2013, under general anesthesia, the patient was subjected to a posterior tumor resection with cervical fixation surgery, and postoperative biopsy was prompted: malignant lymphoma and diffuse large B cell lymphoma invaded the striated muscle. The immunohistochemistry results were NSE (−), S100 (−), GFAP (+), BCL-2 (+), BCL-6 (+), CD20 (++), CD79a (scattered positive), CD45LCA (++), CD8 (scattered positive), ki67 (20% positive), CD5 (+), Pax-5 (+), CD19 (+), CD45RA (part-positive), and MUM-1 (−).

The patient was then treated with chemotherapy in our hospital and followed-up. Pictures C–F are the latest postoperative follow-up images: Enhanced T_1W image with HiBW (C) shows some metal artifacts on the level of C3 vertebral, as indicated by the blue arrow. In addition, the spinal cord is observed. However, the metal artifacts in the images D–F, which were imaged with T_1W using SEMAC and VAT, were narrower than in the images taken without these techniques, such as image C. The spinal cord and other intraspinal structures (green arrow), paraspinal soft tissues can be more clearly imaged.

Images A and B in Figure 4 are 2 T_1W images acquired using a HiBW acquisition sequence with or without SEMAC. They are located at the field of view margin slice of the metal implants, as indicated by the yellow line marked in picture C. The SEMAC factor was still 8, that is, there were 8 slices in addition to the center, which was used mathematically to correct the distortion artifacts through the plane. However, the area of artifacts in image B is not significantly reduced compared to A. Nevertheless, SEMAC can display more details of the prosthesis, such as the pedicle screw (green arrows), which is indicated clearly in B, whereas the traditional common HiBW technology does not show these details.

Figure 5 presents a case of a plasma lymphoma patient after surgery. Picture A is an optimized HiBW image, and images B and C are T_2W and T_1W images, respectively, which were all acquired using SEMAC. There were decreased artifacts in images B and C compared to A, and an irregular-shaped tumor was observed in the sacral canal. Picture F is the mask of the T_1W image, after gadolinium injection. The subtraction of E and F can observe such that the tumor is significantly enhanced, and adjacent soft tissues of internal fixation showed enhancement considering the tumor recurrence and invasion paraspinal soft tissues.

4. Discussion

The spinal fixation technique is now widely used in the treatment of spinal degenerative disease, tumors, traumas, and other
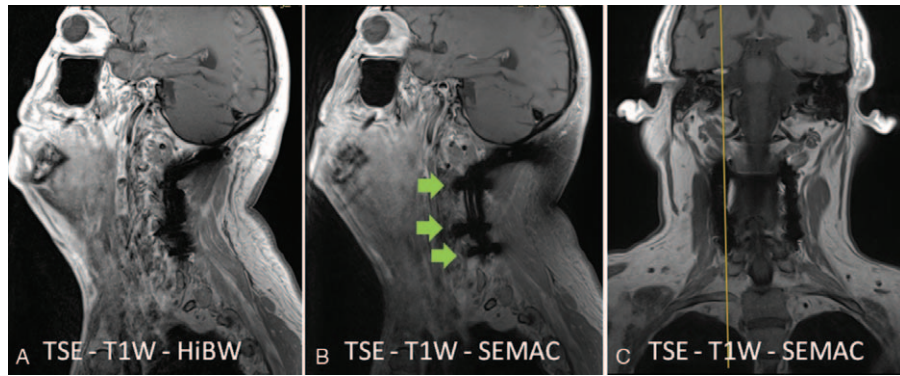
Figure 4. Pictures A and B are 2 T_1 weighted images acquired using the high-bandwidth acquisition sequence with or without slice-encoding metal artifact correction. They are located at the field of view margin slice of the metal implants, as indicated by the yellow line marked in picture C. The area of artifacts in B is not significantly reduced compared to A, but the slice-encoding metal artifact correction better displayed more details of the prosthesis, as shown by the green arrows.

infections, and the most common used is the pedicle screw fixation system.[17] However, in practice, many factors may lead to a poor fixed position or even failure and may lead to some complications.[1] Thus, a more accurate assessment tool is urgently needed to properly evaluate the internal fixation and peripheral soft tissues, thereby providing more accurate imaging data for the determination of successive treatment. MRI is 1 technique with a large potential for the assessment of the metal and surrounding tissue conditions.

Spinal fixation techniques have achieved significant progress with the development of spinal biomechanics and materials science. Titanium material is widely used as an implantation prosthesis due to its good biocompatibility. Furthermore, there are no significant ferromagnetism and thermal magnetic effects,

and patients with titanium prostheses can be safely examined in clinical MR scanners, which may not cause the implantation to move in the body and may not produce heat that injures the tissues. In our study, 27 patients had no complaints on discomfort during the entire MRI examination. Thus, the fixed titanium alloy is safe for humans under the 3 T scanner, as concluded by previous reports on 3 T scanners.

In recent years, a number of teams have developed novel MRI techniques to reduce metal artifacts,[18] and many achievements had been expected to put into clinical use.[19–22] Sequence-based methods, such as SEMAC and VAT, combined with HiBW acquisition methods are aimed at controlling and resolving the distortions through-plane and in-plane. Starting from traditional high-bandwidth acquisition technology for reducing artifacts, we
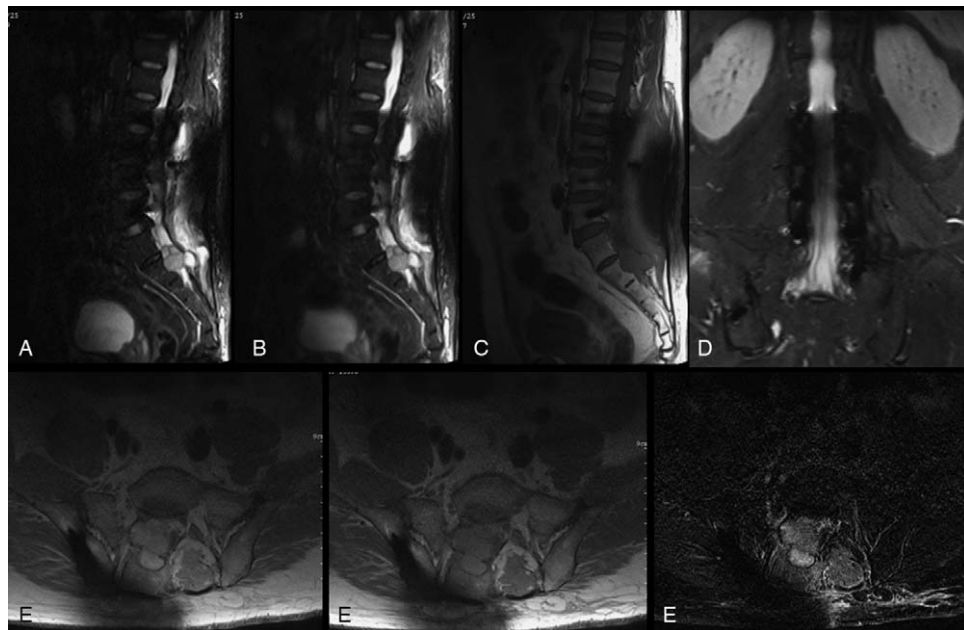
Figure 5. This is another case of a patient with plasmablastic lymphoma who was subjected to magnetic resonance imaging scanning for recurrence assessment. Picture A is an optimized clinical high bandwidth image. Pictures B and C are T_2 weighted and T_1 weighted images, respectively, which were all acquired using magnetic resonance imaging. Vertebral canal and caudal equine can be observed in Picture D. After injection with gadolinium diethylene triamine pentacetic acid, the subtraction of E and F (as shown in G) indicates that the tumors and adjacent soft tissues were significantly enhanced, which should be used to determine the tumor recurrence and invasion.

applied SEMAC and VAT to 27 cases of patients, the results of which were compared to those obtained with conventional sequences with HiBW, but without SEMAC and VAT techniques. According to these results, the pedicle screw artifacts with SEMAC and VAT have been reduced significantly compared to those with conventional technologies.

The visibility of the metal and structures surrounding the implant, such as the dura, spinal cord, intervertebral foramens, nerve roots, bone-implant surface and paraspinal soft tissues, was increased using the SEMAC/VAT correction. In particular, the distinct visualization of the nerve roots between the upper and lower screws can fully explain the role of VAT and SEMAC in the reduction of artifacts in-plane and through-plane. The 2 radiologists performed a semi-quantitative assessment and showed that **the novel techniques of SEMAC-VAT may be a predominant clinical MRI tool** in the evaluation of the spinal implant and peripheral soft tissues.

Fat suppression is frequently used in MR imaging to suppress adipose tissue signal and enhance the detection of pathological tissues. Among various fat suppression methods, chemical shift-selective fat saturation is recommended in the presence of large amounts of adipose tissue and is commonly used in spinal MR imaging. Lee[18] found that SEMAC correction in fat-saturated T_2-W MR images led to significantly greater reductions in the metallic artifacts. However, the signal pile-up could not be completely corrected. The main limitation of spectral fat saturation is the sensitivity to the magnetic field in homogeneity in particular when caused by susceptibility artifacts near metallic implants. In this study, we used a STIR-prepared T_2-W TSE sequences for fat suppression to improve the visibility of implants and soft tissue lesions. According to our results, STIR-prepared fat suppression provides more robust reduction of fat signal and a high-quality contrast for the evaluation of bone marrow and other soft tissue lesions surrounding the prosthesis. In Figure 2, after the use of antibiotics, the exudation around the cross connection was significantly reduced. In Figures 3–5, lesions, such as tumors, bone marrow edema, and nerve root sleeve effusion, were clearly observed in STIR with SEMAC-VAT images. **Thus, the STIR fat-suppression T_2W images with SEMAC-VAT correction is expected to play an important role in the diagnosis of lesions, such as tumors, infections, and fresh fractures, which can also be used to assess the lesion progression and therapeutic effect among patients with metallic prosthesis.**

However, among patients with spinal primary or metastasized malignant tumors, the most important assessment after receiving a metallic prosthesis transplantation is to make a diagnosis regarding whether the tumor is a recurrent or new metastasis. As we previously described above, the STIR fat suppression technique is typically used to detect the presence of lesions, but there are still some difficulties regarding making qualitative diagnoses. Thus, it is necessary to inject the contrast agent Ga-DTPA to observe the blood supply of the mass and to perform a comprehensive assessment of recurrence. In our study, Figure 3 shows that the patient was subjected to a posterior cervical vertebral surgery for the invasion of non-Hodgkin lymphoma, and STIR and T_1W enhanced MRI with SEMAC-VAT correction showed no clear soft tissue mass in the postoperative evaluation. Figure 5 shows a patient with a symptom of lower extremity debilitation 6 months later after spinal surgery for plasmablastic lymphoma invasion of the lumbosacral canal. STIR-T_2W with SEMAC prompted sacral canal mass, with the T_1W-SEAMC

subtraction of the pre- and post- Ga-DTPA injection, and the tumor was significantly enhanced. Although we found that in this study, T_1W-SEMAC is best for metal prosthesis visualization, even in the margin of the field of view, and it can provide more details compared to the control group. However, when T_1W-SEMAC was used in contrast-enhancement imaging for cancer diagnosis, it was likely to miss the peak time in these hypervascular tumors because its scan time was excessively long. And the fat suppression techniques such as short inversion recovery or Dixon fat and water separation method on T_1W-SEMAC may be beneficial to increase the contrast between the tumors and the peri-prosthesis soft tissues.

There are some limitations to our research. First, the artifact area was reduced by the application of 2 strategies, but the biases on the qualitative and quantitative evaluation may be unavoidable. Second, the total scanning time of SEMAC was relatively long due to the additional phase-encoding on the slice direction, and this longer scanning time must be compensated for with acceleration strategies (parallel imaging, partial sampling, and increased echo train length) to ensure clinically acceptable scan times. The small number of study objects is another limitation of our study. A subsequent study with more cases will be conducted to obtain a more reliable statistically result.

In conclusion, optimized pulse sequences equipped with SEMAC and VAT were applied for the assessment of spinal metallic endoprostheses, and clinical benefits were demonstrated. These sequences significantly reduced metal artifacts in the qualitative and quantitative analyses and may thus facilitate the follow-up of patients who have undergone spine surgery.

Author contributions

Conceptualization: Shihong Li.
Date curation: Chun Xin, Houdong Liu, Shihong Li, Guangwu Lin.
Formal analysis: Guangwu Lin.
Methodology: Chun Xin, Houdong Liu.
Funding acquisition: Shihong Li.
Software: Shihong Li, Guangwu Lin.
Writing – original draft: Houdong Liu.
Writing – review & editing: Chun Xin.

References

[1] Glassman SD, Carreon LY, Dimar JR, et al. Clinical outcomes in older patients after posterolateral lumbar fusion. Spine J 2007;7:547–51.

[2] Atlas SJ, Keller RB, Wu YA, et al. Long-term outcomes of surgical and nonsurgical management of lumbar spinal stenosis: 8 to 10 year results from the maine lumbar spine study. Spine (Phila Pa 1976) 2005;30:936–43.

[3] Carreon LY, Puno RM, Dimar JR2nd, et al. Perioperative complications of posterior lumbar decompression and arthrodesis in older adults. J Bone Joint Surg Am 2003;85:2089–92.

[4] Raffo CS, Lauerman WC. Predicting morbidity and mortality of lumbar spine arthrodesis in patients in their ninth decade. Spine (Phila Pa 1976) 2006;31:99–103.

[5] Brooks D, Eskander M, Balsis S, et al. Imaging assessment of lumbar pedicle screw placement: sensitivity and specificity of plain radiographs and computer axial tomography. Spine (Phila Pa 1976) 2007;32:1450–3.

[6] Allam Y, Silbermann J, Riese F, et al. Computer tomography assessment of pedicle screw placement in thoracic spine: comparison between free hand and a generic 3D-based navigation techniques. Eur Spine J 2013;22:648–53.

[7] Lu W, Pauly KB, Gold GE, et al. SEMAC: slice encoding for metal artifact correction in MRI. Magn Reson Med 2009;62:66–76.

[8] Kolind SH, Mackay AL, Munk PL, et al. Quantitative evaluation of metal artifact reduction techniques. J Magn Reson Imaging 2004; 20:487–95.

[9] Zho SY, Kim MO, Lee KW, et al. Artifact reduction from metallic dental materials in T1-weighted spin-echo imaging at 3.0 tesla. J Magn Reson Imaging 2013;37:471–8.

[10] Cho ZH, Kim DJ, Kim YK. Total inhomogeneity correction including chemical shifts and susceptibility by view angle tilting. Med Phys 1988;15:7–11.

[11] Lu W, Pauly KB, Gold GE, et al. Slice encoding for metal artifact correction with noise reduction. Magn Reson Med 2011;65:1352–7.

[12] Carl M, Koch K, Du J. MR imaging near metal with undersampled 3D radial UTE-MAVRIC sequences. Magn Reson Med 2013;69: 27–36.

[13] Koch KM, Brau AC, Chen W, et al. Imaging near metal with a MAVRIC-SEMAC hybrid. Magn Reson Med 2011;65:71–82.

[14] Kretzschmar M, Nardo L, Han MM, et al. Metal artefact suppression at 3 T MRI: comparison of MAVRIC-SL with conventional fast spin echo sequences in patients with hip joint arthroplasty. Eur Radiol 2015;25:2403–11.

[15] Lee YH, Lim D, Kim E, et al. Usefulness of slice encoding for metal artifact correction (SEMAC) for reducing metallic artifacts in 3-T MRI. Magn Reson Imaging 2013;31:703–6.

[16] Cha JG, Jin W, Lee MH, et al. Reducing metallic artifacts in postoperative spinal imaging: usefulness of IDEAL contrast-enhanced T1- and T2-weighted MR imaging–phantom and clinical studies. Radiology 2011;259:885–93.

[17] Doulgeris JJ, Aghayev K, Gonzalez-Blohm SA, et al. Biomechanical comparison of an interspinous fusion device and bilateral pedicle screw system as additional fixation for lateral lumbar interbody fusion. Clin Biomech (Bristol, Avon) 2015;30:205–10.

[18] Lee YH, Lim D, Kim E, et al. Feasibility of fat-saturated T2-weighted magnetic resonance imaging with slice encoding for metal artifact correction (SEMAC) at 3T. Magn Reson Imaging 2014;32:1001–5.

[19] Bachschmidt TJ, Sutter R, Jakob PM, et al. Knee implant imaging at 3 Tesla using high-bandwidth radiofrequency pulses. J Magn Reson Imaging 2015;41:1570–80.

[20] Talbot BS, Weinberg EP. MR Imaging with metal-suppression sequences for evaluation of total joint arthroplasty. Radiographics 2016;36: 209–25.

[21] den Harder JC, van Yperen GH, Blume UA, et al. Off-resonance suppression for multispectral MR imaging near metallic implants. Magn Reson Med 2015;73:233–43.

[22] den Harder JC, van Yperen GH, Blume UA, et al. Ripple artifact reduction using slice overlap in slice encoding for metal artifact correction. Magn Reson Med 2015;73:318–24.